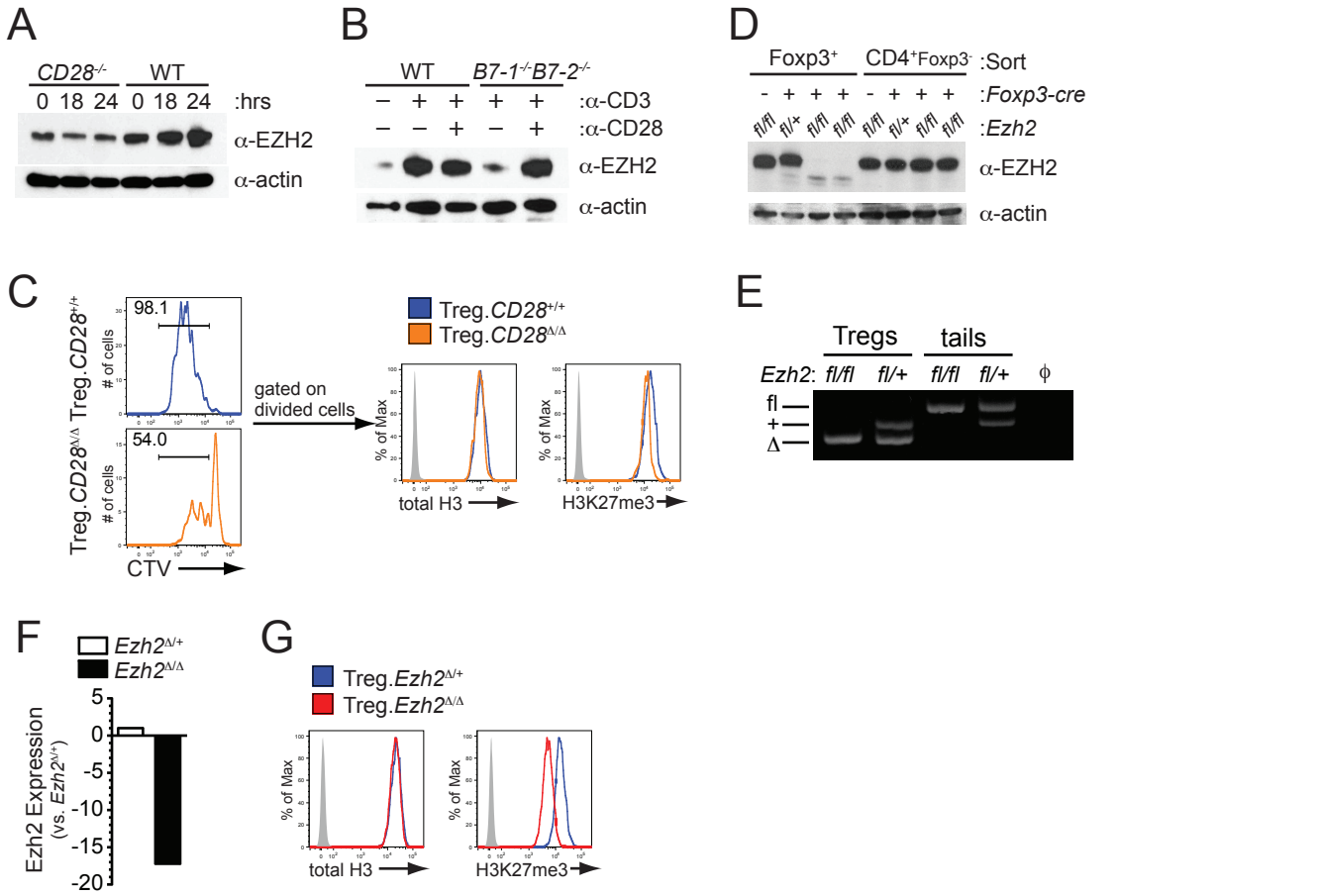

Figure S1 (Related to Figure 1). CD28-dependent expression of Ezh2 in Treg cells.
(A) Ezh2 western blot analysis of CD4$^+$ T cells from CD28-deficient or WT mice at 0, 18, or 24 hours after stimulation with anti-CD3 and anti-CD28 antibody-coated beads.
(B) Ezh2 western blot analysis of CD4$^+$ T cells purified from whole lymphocyte cultures of WT or B7-1 and B7-2-deficient cells (B7-1$^{-/-}$B7-2$^{-/-}$) stimulated with soluble anti-CD3 or anti-CD3 and anti-CD28 antibodies for 24 hours. Because activation of CD4$^+$ T cells with soluble anti-CD3 antibodies presented on cells only lacking CD28 costimulatory ligands using B7-1$^{-/-}$B7-2$^{-/-}$ mice abrogated the induction of Ezh2 protein, CD28 stimulation by B7 molecules is the essential costimulatory molecule for inducing Ezh2.
(C) Comparison of H3K27me3 and total-H3 staining between sorted populations of Treg cells from Foxp3-cre x CD28$^{fl/+}$ or CD28$^{fl/fl}$ mice three days after activation with anti-CD3 and anti-CD28 antibody-coated beads (right). The histogram plots of H3K27me3 and total-H3 staining only depict dividing cells by first gating on cells that diluted the CTV dye (gating strategy depicted in left plots). Isotype control antibody staining in gray. Data is representative of three independent experiments.
(D – G) Specificity of Ezh2 disruption in Treg cells:
(D) Ezh2 western blot analysis of sorted Treg cells or CD4$^+$ T cells activated in culture for three days from four mice with indicated genotypes for Foxp3-cre and Ezh2^{fl}.
(E) Genomic PCR to assess recombination of Ezh2^{fl} allele to Ezh2$^{\Delta}$ allele in DNA from sorted Treg cells or tails from same mice with indicated Ezh2 genotypes, φ = no DNA control.
(F) Quantitative PCR analysis for expression of Ezh2 from freshly sorted CD62L^{hi} Treg cells from Foxp3-cre;Ezh2$^{fl/fl}$ (Ezh2$^{\Delta/\Delta}$) and Foxp3-cre;Ezh2$^{fl/+}$ (Ezh2$^{\Delta/+}$) mice (Taqman probe Mm00468464_m1, spanning floxed exons 19 to 20).
(G) Comparison of H3K27me3 and total-H3 staining between sorted populations of Treg cells from Foxp3-cre x Ezh2$^{fl/+}$ or Ezh2$^{fl/fl}$ mice three days after activation with anti-CD3 and anti-CD28 antibody-coated beads. Isotype control antibody staining in gray. Data is representative of five independent experiments.

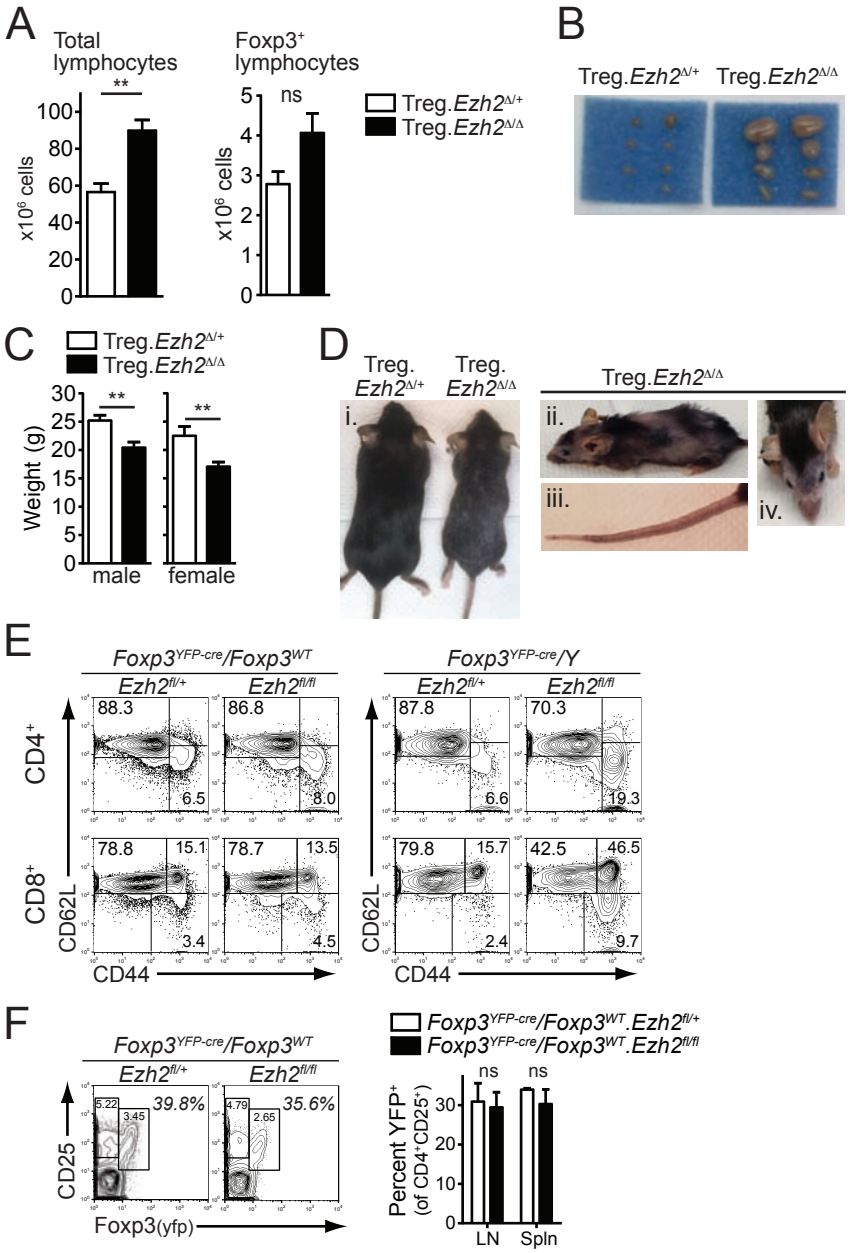

Figure S2 (Related to Figure 3). Autoimmune phenotypes in Treg.Ezh2Δ/Δ mice.

(A) Total lymphocyte counts (left) or Foxp3$^+$ cells (from lymph nodes only) per mouse from 6 to 8 week old mice (mean ±SEM, n=6 mice per group).

(B) Representative picture of lymph nodes from 24 to 30 week old Treg.Ezh2$^{\Delta/+}$ and Treg.Ezh2$^{\Delta/\Delta}$ mice (30 week old mice depicted).

(C) Weight of male and female Treg.Ezh2$^{\Delta/+}$ versus Treg.Ezh2$^{\Delta/\Delta}$ mice aged 14 weeks (mean ±SEM, n= 5-9 mice per group).

(D) Representative pictures of Treg.Ezh2$^{\Delta/+}$ and Treg.Ezh2$^{\Delta/\Delta}$ mice showing: i. reduced size and loss of hair pigmentation, ii. hair loss, iii. scaly tail, and iv. swelling around eyes.

(E) Analysis of CD4$^+$ and CD8$^+$ T cell activation in lymph nodes by CD44 and CD62L expression in female Foxp3$^{YFP\text{-}cre}$/Foxp3^{WT};Ezh2$^{fl/+}$ versus Foxp3$^{YFP\text{-}cre}$/Foxp3^{WT};Ezh2$^{fl/fl}$ mice (representative of mice aged 8 to 37 weeks old, 14 week old mice shown) revealed no difference in CD4$^+$ or CD8$^+$ T cell activation in the presence of Ezh2-deficient Treg cells (on left). In contrast (on right), CD4$^+$ and CD8$^+$ T cells from male Foxp3$^{YFP\text{-}cre}$/Y;Ezh2$^{fl/fl}$ mice exhibited increased T cell activation when compared to Foxp3$^{YFP\text{-}cre}$/Y;Ezh2$^{fl/+}$ littermates (16 week old mice shown). Data is representative of at least three mice per genotype.

(F) Representative plots showing the percentage (%) of Foxp3YFP-cre-expressing Treg cells of all CD25$^+$ Treg cells in lymph nodes of Foxp3$^{YFP\text{-}cre}$/Foxp3^{WT};Ezh2$^{fl/+}$ versus Foxp3$^{YFP\text{-}cre}$/Foxp3^{WT};Ezh2$^{fl/fl}$ mice (left) and cumulative results from lymph nodes (LN) and spleens (Spln) (right, mean ±SEM from 3-4 mice per genotype).

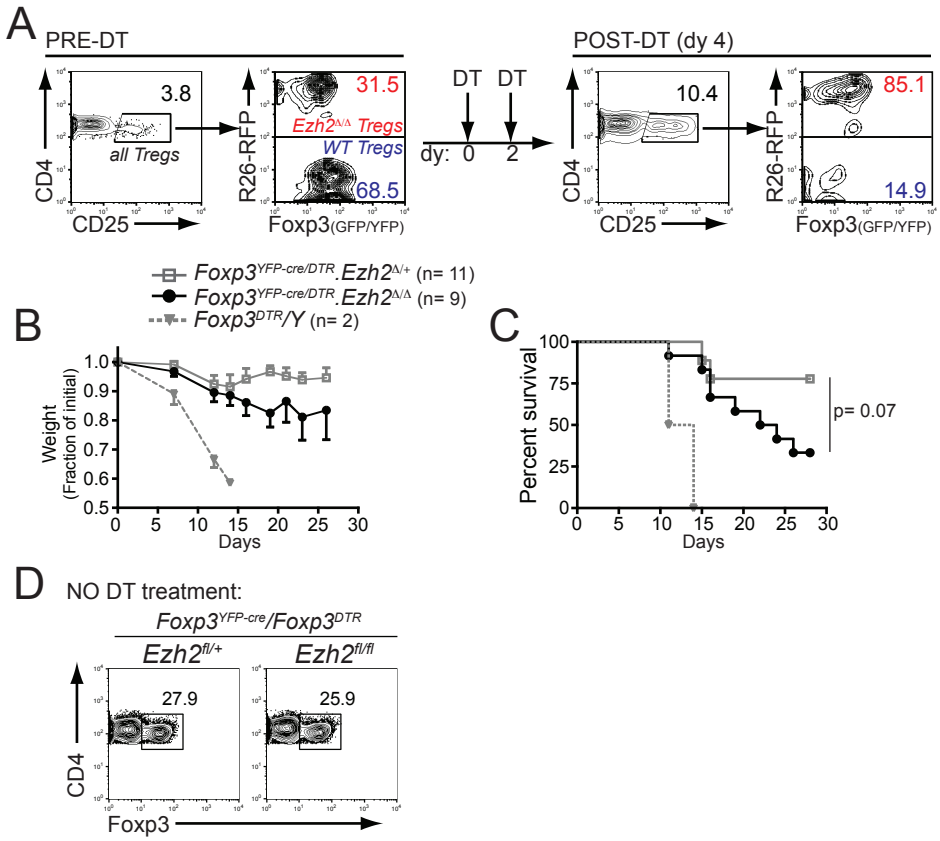

Figure S3 (related to Figure 4). Acute depletion of wild type Treg cells in adult mice reveals Ezh2-deficient Treg cells are unable to prevent autoimmune disease.

(A) Depletion of wild type Treg cells in a Foxp3$^{YFP\text{-}cre}$/Foxp3^{DTR};Ezh2$^{fl/fl}$;R26$^{LSL\text{-}RFP}$ adult mouse after two doses of DT was confirmed by analysis of the blood pre- and post-treatment (day 4) for YFP^{+}RFP^{+} (Foxp3YFP-cre-expressing) cells.

(B and C) Weight (B) and survival (C) of indicated mice treated with DT three times per week for up to four weeks. Foxp3^{DTR}/Y mice that completely deplete all Treg cells with DT treatment served as positive controls for disease induction. Cumulative results from two independent experiments are shown.

(D) Representative flow cytometric analysis of the percentage of Foxp3^{+} Treg cells (of CD4+ cells) in spleens of Foxp3$^{YFP\text{-}cre}$/Foxp3^{DTR};Ezh2$^{fl/+}$ or Foxp3$^{YFP\text{-}cre}$/Foxp3^{DTR};Ezh2$^{fl/fl}$ mice that were not treated with DT.

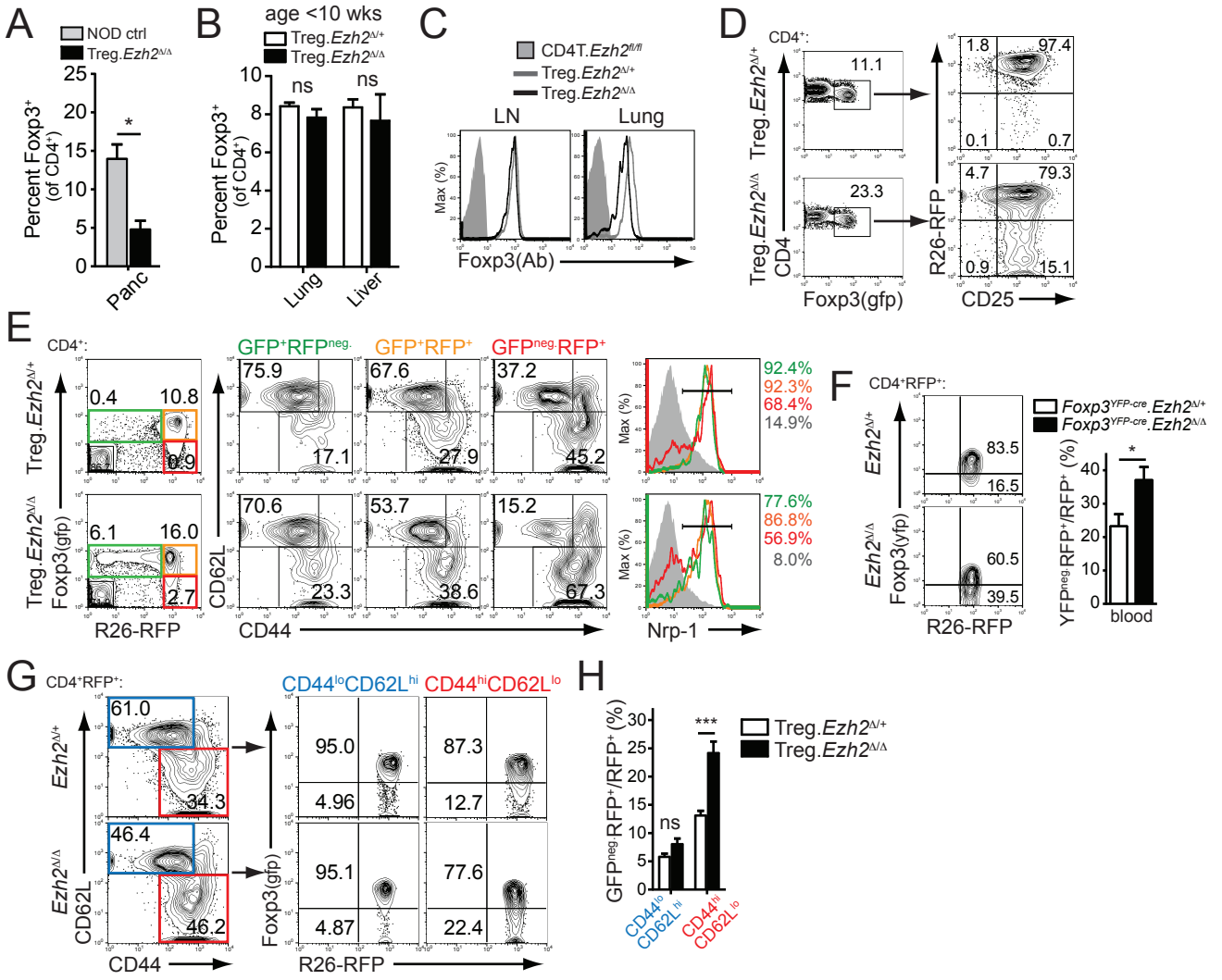

Figure S4 (related to Figure 5). Lineage tracing and Foxp3 destabilization of activated Ezh2-defiecient Treg cells.
(A) Quantification of the frequencies of Treg cells (as percentage of Foxp3+ cells of CD4+ cells) from the pancreas of NOD (Ezh2$^{+/+}$) and Treg.Ezh2$^{\Delta/\Delta}$ mice 15 to 30 weeks old. Comparison to NOD mice was performed because no T cells were detectable in the pancreas of Treg.Ezh2$^{\Delta/+}$ mice.
(B) Quantification of the frequency of Treg cells (as percentage of Foxp3+ cells of CD4+ T cells) from lung and liver of mice 8-10 weeks old (n= 4 mice/ genotype from two experiments). Thus, younger mice exhibit no defect in Treg cell frequency in tissues prior to the development of autoimmune phenotypes with age.
(C) Representative Foxp3 expression by Foxp3 antibody staining of CD4^{+}CD25^{+} populations from the lymph node and lung of indicated mice.
(D) Analysis of CD4^{+}Foxp3^{+} cells from peripheral lymph nodes for CD25 and RFP expression showed that the GFP^{+}RFP$^{neg.}$ (newly Foxp3-expressing) cells are CD25^{+}, indicative of committed Treg cells as reported by Miyao et al. (2012).
(E) GFP^{+}RFP$^{neg.}$ (newly Foxp3-expressing) cells in peripheral lymph nodes have characteristics of thymically derived Treg cells: CD44 and CD62L expression in different populations of the Treg lineage showed GFP^{+}RFP$^{neg.}$ cells were more naïve than stable (GFP^{+}RFP^{+}) or destabilized (GFP$^{neg.}$RFP^{+}) Treg cells. GFP^{+}RFP$^{neg.}$ cells expressed Nrp-1 (comparable to stable GFP^{+}RFP^{+} Treg cells), a marker of Treg cells derived from the thymus. Solid gray histogram depicts CD4^{+}GFP$^{neg.}$RFP$^{neg.}$ cells.
(F) Analysis of blood from Foxp3$^{YFP\text{-}cre}$/Foxp3^{WT};Ezh2$^{fl/+}$ or Foxp3$^{YFP\text{-}cre}$/Foxp3^{WT};Ezh2$^{fl/fl}$ female mice for the presence of YFP$^{neg.}$RFP^{+} cells. Representative flow cytometric data (left) and cumulative data of mean ±SEM from 9-10 mice per genotype (right).
(G) CD4^{+}RFP^{+} cells from peripheral lymph nodes of Treg.Ezh2$^{\Delta/+}$ or Treg.Ezh2$^{\Delta/\Delta}$ mice were divided into populations of CD44^{lo}CD62L^{hi} (blue) or CD44^{hi}CD62L^{lo} (red) (on left) and then analyzed for the percentage of GFP$^{neg.}$RFP^{+} cells in each population (on right).
(H) Quantification of the percentage of GFP$^{neg.}$RFP^{+} cells in each population in (G), mean ±SEM from 6-10 mice per genotype.

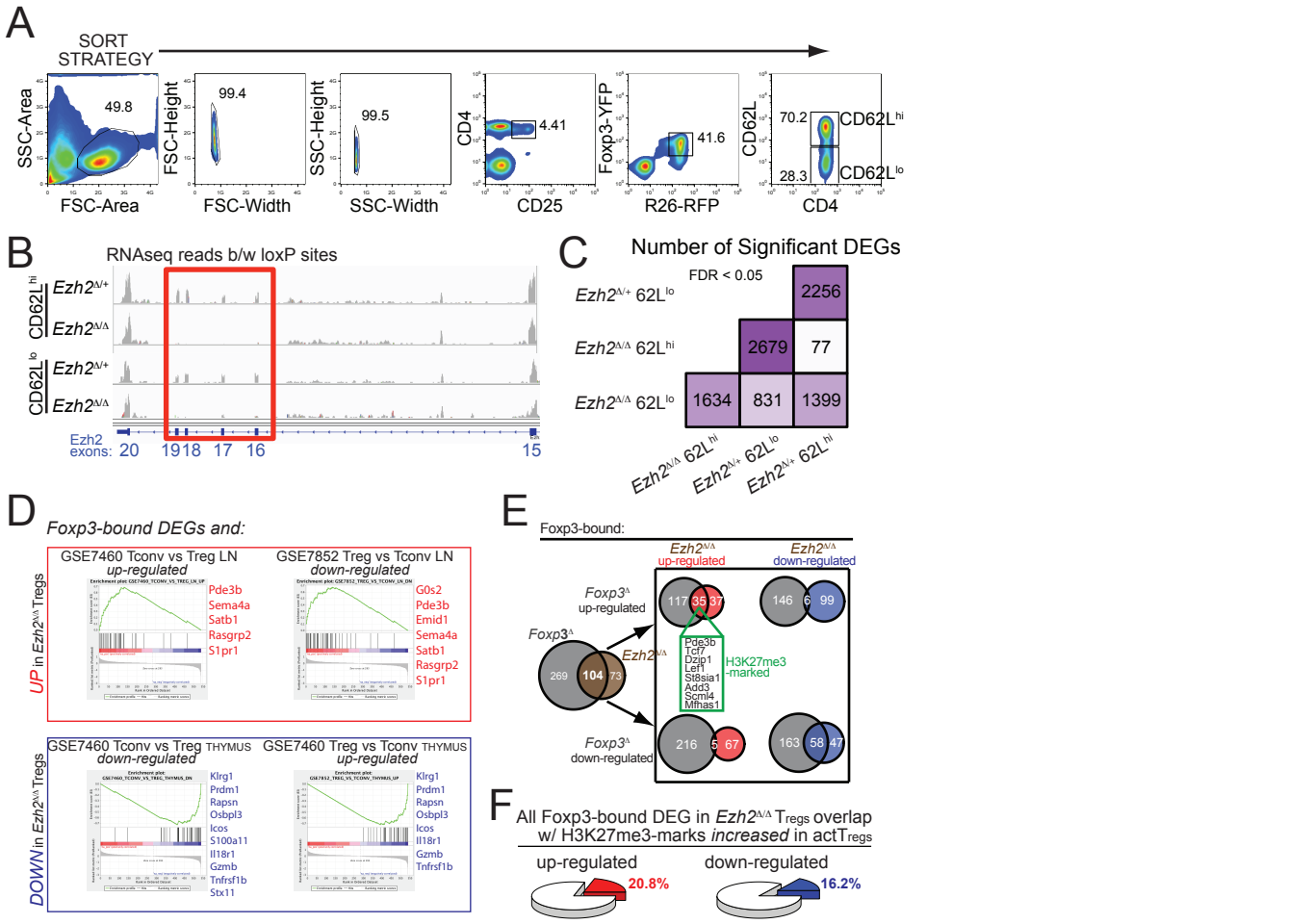

Figure S5 (related to Figure 6). Gene expression analysis of Ezh2-defiecient Treg cells.

(A) Sort strategy (from left to right) for purifying populations of CD62L^{hi} versus CD62L^{lo} Treg cells that maintain Ezh2 (Ezh2$^{\Delta/+}$) or are deficient for Ezh2 (Ezh2$^{\Delta/\Delta}$) from lymph nodes and spleens of Foxp3$^{YFP\text{-}cre}$/Foxp3^{WT};Ezh2$^{fl/+}$ or Foxp3$^{YFP\text{-}cre}$/Foxp3^{WT};Ezh2$^{fl/fl}$ female mice, respectively.

(B) RNAseq reads mapped at the Ezh2 locus (exons 15-20 shown) confirms the complete deletion of exons 16-19 (exons between the engineered loxP sites) in both CD62L^{hi} and CD62L^{lo} Ezh2$^{\Delta/\Delta}$ Treg cells.

(C) Number of significantly differentially expressed genes (DEGs) shown for each pairwise comparison between Ezh2$^{\Delta/\Delta}$ CD62L^{hi}, Ezh2$^{\Delta/\Delta}$ CD62L^{lo}, Ezh2$^{\Delta/+}$ CD62L^{hi}, Ezh2$^{\Delta/+}$ CD62L^{lo} Treg cells. A total of 3,097 DEGs from all comparisons (FDR < 0.05) and 831 DEGs between Ezh2$^{\Delta/\Delta}$ CD62L^{lo} vs. Ezh2$^{\Delta/+}$ CD62L^{lo} (termed Ezh2$^{\Delta/\Delta}$). Noteably, only 77 DEGs exist between Ezh2$^{\Delta/\Delta}$ CD62L^{hi} and Ezh2$^{\Delta/+}$ CD62L^{hi} cells.

(D) Gene set enrichment analysis (GSEA) in C7 immunological signatures set in MSigDB for DEGs that are Foxp3-bound between Ezh2$^{\Delta/\Delta}$ vs. Ezh2$^{\Delta/+}$ Treg cells indicated that Ezh2-deficient Treg cells have a transcriptional fingerprint similar to conventional T cells when compared to normal Treg cells. Top two hits in GSEA are shown for genes either up-regulated (red box) or down-regulated (blue box) in Ezh2$^{\Delta/\Delta}$ Treg cells. The genes listed on the right in red or blue text were the top rank-ordered genes with Log2FC ≥ 0.5. The majority of genes identified by GSEA here were also identified in our comparison of Foxp3$^{\Delta}$ and Ezh2$^{\Delta/\Delta}$ Treg cells (marked by * in Figure 6E), indicating a strong correlation between genes regulated by the Foxp3 transcriptional program and genes that differentiate conventional T cells and Treg cells. Importantly, Ezh2 regulates these genes.

(E) Related to Figure 6F: left, overlap in Foxp3-bound DEGs in Foxp3$^{\Delta}$ and Ezh2$^{\Delta/\Delta}$ Treg cells (number of genes is shown in white text); middle and right, overlap in Foxp3-bound genes after splitting into DEGs up-regulated (top) or down-regulated (bottom) for comparison of both datasets; green box, H3K27me3 marked genes in activated Treg cells that are bound by Foxp3 and up-regulated in Foxp3$^{\Delta}$ and Ezh2$^{\Delta/\Delta}$ Treg cells.

(F) The percentage of up-regulated (left) or down-regulated (right) Foxp3-bound DEGs in Ezh2$^{\Delta/\Delta}$ that are associated with increased H3K27me3 marks in activated versus resting WT Treg cells.

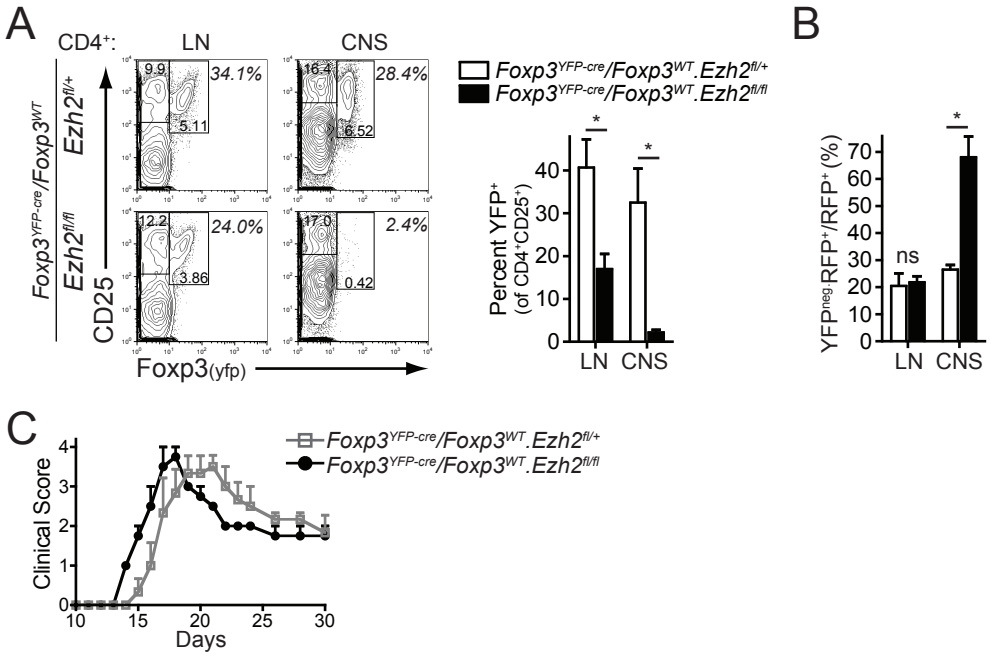

Figure S6 (related to Figure 7). Ezh2-deficient Treg cells are at a competitive disadvantage against wild type Treg cells after acute induction of autoimmune disease.

(A – C) EAE was induced in Foxp3$^{YFP\text{-}cre}$/Foxp3^{WT};Ezh2$^{fl/+}$ or Foxp3$^{YFP\text{-}cre}$/Foxp3^{WT};Ezh2$^{fl/fl}$ female mice (cumulative data from at least three mice per genotype in two independent experiments):

(A) Representative plots showing the percentage (%) of Foxp3YFP-cre-expressing Treg cells of all CD25^{+} Treg cells in lymph nodes (LN) or CNS (left) at 25 to 30 days post induction of EAE and the cumulative results (right).

(B) Percentage of YFP$^{neg.}$RFP^{+} cells generated from Foxp3YFP-cre-expressing Treg cells in lymph nodes (LN) or CNS in indicated mice.

(C) Plot of clinical score versus time (days) after induction of experimental autoimmune encephalomyelitis (EAE) in indicated mice.

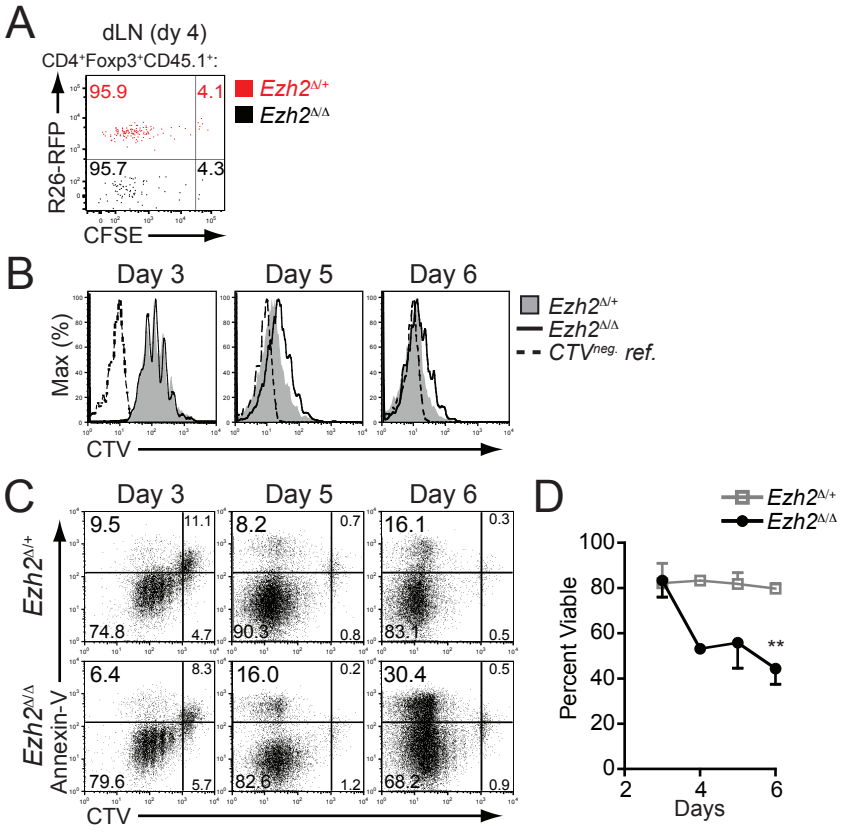

Figure S7 (related to Figure 7). Proliferation and survival of Ezh2-deficient Treg cells.
(A) Ezh2$^{\Delta/+}$ and Ezh2$^{\Delta/\Delta}$ Treg cells (sorted from 2D2^{+};CD4-cre;Ezh2$^{fl/+}$;R26$^{LSL\text{-}RFP}$;CD45.1^{+} or 2D2^{+};CD4-cre;Ezh2$^{fl/fl}$;R26^{WT};CD45.1^{+}, respectively) were labeled with CFSE and co-transferred into MOG+CFA primed CD45.1$^{neg.}$ wild type mice. Four days after transfer, CD4^{+}Foxp3^{+}CD45.1^{+} cells were analyzed for CFSE dilution and RFP expression was used to distinguish Ezh2$^{\Delta/+}$ from Ezh2$^{\Delta/\Delta}$ Treg cells. Results are representative of three independent experiments.
(B and C) Flow cytometric analysis of CTV dilution (B) or CTV versus Annexin V staining (C) in sorted Treg cells from indicated mice 3, 5, or 6 days after stimulation with anti-CD3 and anti-CD28 antibody coated beads (dotted line, CTV unlabeled reference). Representative of three or more independent experiments.
(D) Viability of Treg cells by exclusion of viability dye and monitored by flow cytometry on given days. Data is the cumulative mean ±SEM from 3-5 paired experiments.

Table S1 (related to Figure 6). Summary of key differentially expressed genes in RNAseq dataset comparisons.

Each tab within the excel sheet shows DEGs between comparison of the four different samples analyzed: $Ezh2^{\Delta/\Delta}$ $CD62L^{hi}$, $Ezh2^{\Delta/\Delta}$ $CD62L^{lo}$, $Ezh2^{\Delta/+}$ $CD62L^{hi}$, $Ezh2^{\Delta/+}$ $CD62L^{lo}$ Treg cells. 'KO' refers to $Ezh2^{\Delta/\Delta}$ Treg cells, 'Het' refers to $Ezh2^{\Delta/+}$ Treg cells, 'hi' refers to $CD62L^{hi}$ sorted Treg cells, and 'lo' refers to $CD62L^{lo}$ sorted Treg cells. A complete list of "de-repressed" genes (ie genes with increased expression in activated $Ezh2^{\Delta/\Delta}$ Treg cells) from Figure 6B and a complete list of the 341 overlapping genes between $Foxp3^{\Delta}$ and $Ezh2^{\Delta/\Delta}$ Treg cells from Figure 6E are shown.

SUPPLEMENTAL EXPERIMENTAL PROCEDURES

Mice. *CD28*$^{-/-}$ mice (Shahinian et al., 1993) and wild type mice backcrossed to the NOD background (Figure S1A) and B7-1$^{-/-}$ and B7-2$^{-/-}$ double knock-out mice (Borriello et al., 1997) in a C57BL/6 background were used for Ezh2 protein expression with activation of conventional CD4^{+} T cells. Lineage-tracing utilized the *R26*$^{LSL\text{-}RFP}$ Cre-activated reporter (Luche et al., 2007).

Flow cytometry for H3, H3K27me3, and viability. Cells were first fixed with 3.9% formaldehyde followed by permeabilizing with ice cold 50% methanol in PBS and then washed and stained in 0.5% BSA in PBS with the anti-H3K27me3 and anti-total-H3 monoclonal antibodies (C36B11 and D1H2, respectively, Cell Signaling Technology). Viability was assessed by exclusion of cell impermeable dyes in all *in vitro* assays and analyses of non-lymphoid tissues (LIVE/DEAD Fixable Dead Cell Stain, Invitrogen). Annexin V stain performed as instructed using binding buffer provided (eBiosciences).

Transcriptome data analysis. The FastQC program (http://www.bioinformatics.babraham.ac.uk/projects/fastqc) was used for a quality check. The differential gene expression analysis of RNAseq was done using TopHat and Cufflinks (Trapnell et al., 2012). Briefly, TopHat (http://tophat.cbcb.umd.edu/)(Trapnell et al., 2009) was used to align RNAseq reads against the mouse genome build mm10, downloaded via the UCSC genome browser. Cufflinks (http://cufflinks.cbcb.umd.edu/)(Trapnell et al., 2010) was used to assemble the reads into transcripts, and Cuffdiff analyzed genes and transcripts differentially

expressed using a rigorous statistical analysis between groups. Principal component analysis (PCA) was performed on gene expression data represented as Fragments Per Kilobase of transcript per Million mapped reads (FPKM) values obtained from Cufflinks program using the FactoMineR (R package for multivariate data analysis) (Lê et al., 2008), which maximizes the variance of the projected points.

Microarray data analysis. All microarrays were normalized using GeneChip Robust Multiarray Averaging (GC-RMA), and differential expression was estimated using the limma package in Bioconductor (Gentleman et al., 2004; Smyth, 2004). Moderated *t*-statistics, B statistics, false-discovery rates and *P* values were computed for each gene for the comparison of interest. Genes were considered differentially expressed if they had a q value <0.05 after Benjamini-Hochberg FDR estimation. Publically available data from GEO with accession number GSE40685 was used to compare differential expression between $Foxp3^{gfpKO}$ Treg vs. WT Treg and GSE39594 was used to compare differentially expressed genes between human naïve $CD4^+$ T cells that were unstimulated, stimulated with anti-CD3, or stimulated with anti-CD3 and anti-CD28 for 24 hours.

Genome-wide analysis of Foxp3 and H3K27me3 binding sites. ChIP-seq data for Foxp3 was obtained from Gavin et al. (2007) to identify Foxp3 binding sites (GSE40684). H3K27me3 marks increased in activated Treg cells (aTreg cells) compared to resting Treg cells (rTreg cells) were identified from Arvey et al. (2014) (GSE55773). The resulting bed-formatted files were imported into the ChIPpeakAnno

package (Zhu et al., 2010) in R/BioConductor for peak annotation analysis. The two-sample Kolmogorov-Smirnov (K-S) statistical test was used to determine the significance of the shift between the curves in the cumulative distribution plot.

Gene set enrichment analysis. Enrichment for C7 immunological signatures set in the Molecular Signatures Database (MSigDB) was computed by running GSEA (Mootha et al., 2003; Subramanian et al., 2005) against all differentially expressed genes bound by Foxp3 based on the fold-change ranked list for *Ezh2*$^{\Delta/\Delta}$ CD62L^{lo} vs *Ezh2*$^{\Delta/+}$ CD62L^{lo} Treg cells.

SUPPLEMENTAL REFERENCES

Borriello, F., Sethna, M.P., Boyd, S.D., Schweitzer, A.N., Tivol, E.A., Jacoby, D., Strom, T.B., Simpson, E.M., Freeman, G.J., and Sharpe, A.H. (1997). B7-1 and B7-2 have overlapping, critical roles in immunoglobulin class switching and germinal center formation. Immunity *6*, 303-313.

Gentleman, R.C., Carey, V.J., Bates, D.M., Bolstad, B., Dettling, M., Dudoit, S., Ellis, B., Gautier, L., Ge, Y., Gentry, J.*, et al.* (2004). Bioconductor: open software development for computational biology and bioinformatics. Genome Biol *5*, R80.

Lê, S., Josse, J., and Husson, F. (2008). FactoMineR: an R package for multivariate analysis. Journal of Statistical Software *25*, 1-18.

Luche, H., Weber, O., Nageswara Rao, T., Blum, C., and Fehling, H.J. (2007). Faithful activation of an extra-bright red fluorescent protein in "knock-in" Cre-reporter mice ideally suited for lineage tracing studies. Eur J Immunol *37*, 43-53.

Mootha, V.K., Lindgren, C.M., Eriksson, K.F., Subramanian, A., Sihag, S., Lehar, J., Puigserver, P., Carlsson, E., Ridderstrale, M., Laurila, E.*, et al.* (2003). PGC-1alpha-responsive genes involved in oxidative phosphorylation are coordinately downregulated in human diabetes. Nature genetics *34*, 267-273.

Shahinian, A., Pfeffer, K., Lee, K.P., Kundig, T.M., Kishihara, K., Wakeham, A., Kawai, K., Ohashi, P.S., Thompson, C.B., and Mak, T.W. (1993). Differential T cell costimulatory requirements in CD28-deficient mice. Science *261*, 609-612.

Smyth, G.K. (2004). Linear models and empirical bayes methods for assessing differential expression in microarray experiments. Stat Appl Genet Mol Biol *3*, Article3.

Subramanian, A., Tamayo, P., Mootha, V.K., Mukherjee, S., Ebert, B.L., Gillette, M.A., Paulovich, A., Pomeroy, S.L., Golub, T.R., Lander, E.S., and Mesirov, J.P. (2005). Gene set enrichment analysis: a

knowledge-based approach for interpreting genome-wide expression profiles. Proceedings of the National Academy of Sciences of the United States of America *102*, 15545-15550.

Trapnell, C., Pachter, L., and Salzberg, S.L. (2009). TopHat: discovering splice junctions with RNA-Seq. Bioinformatics *25*, 1105-1111.

Trapnell, C., Roberts, A., Goff, L., Pertea, G., Kim, D., Kelley, D.R., Pimentel, H., Salzberg, S.L., Rinn, J.L., and Pachter, L. (2012). Differential gene and transcript expression analysis of RNA-seq experiments with TopHat and Cufflinks. Nat Protoc *7*, 562-578.

Trapnell, C., Williams, B.A., Pertea, G., Mortazavi, A., Kwan, G., van Baren, M.J., Salzberg, S.L., Wold, B.J., and Pachter, L. (2010). Transcript assembly and quantification by RNA-Seq reveals unannotated transcripts and isoform switching during cell differentiation. Nat Biotechnol *28*, 511-515.

Zhu, L.J., Gazin, C., Lawson, N.D., Pages, H., Lin, S.M., Lapointe, D.S., and Green, M.R. (2010). ChIPpeakAnno: a Bioconductor package to annotate ChIP-seq and ChIP-chip data. BMC Bioinformatics *11*, 237.